

# Nanosecond Tracer Diffusion as a Probe of the Solution Structure and Molecular Mobility of Protein Assemblies: The Case of Ovalbumin

Christian Beck,<sup>†,‡,§</sup> Marco Grimaldo,<sup>†</sup> Felix Roosen-Runge,<sup>§</sup> Michal K. Braun,<sup>‡,§</sup> Fajun Zhang,<sup>‡,§</sup> Frank Schreiber,<sup>‡</sup> and Tilo Seydel<sup>\*,†,§</sup>

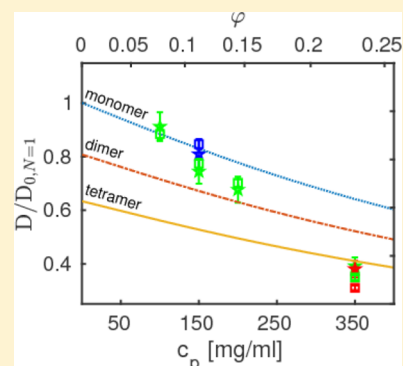
<sup>†</sup>Institut Max von Laue—Paul Langevin (ILL), B.P.156, F-38042 Grenoble, France

<sup>‡</sup>Institut für Angewandte Physik, Universität Tübingen, Auf der Morgenstelle 10, 72076 Tübingen, Germany

<sup>§</sup>Division of Physical Chemistry, Department of Chemistry, Lund University, Naturvetarvägen 16, SE-22100 Lund, Sweden

## Supporting Information

**ABSTRACT:** Protein diffusion is not only an important process ensuring biological function but can also be used as a probe to obtain information on structural properties of protein assemblies in liquid solutions. Here, we explore the oligomerization state of ovalbumin at high protein concentrations by means of its short-time self-diffusion. We employ high-resolution incoherent quasielastic neutron scattering to access the self-diffusion on nanosecond timescales, on which interparticle contacts are not altered. Our results indicate that ovalbumin in aqueous (D<sub>2</sub>O) solutions occurs in increasingly large assemblies of its monomeric subunits with rising protein concentration. It changes from nearly monomeric toward dimeric and ultimately larger than tetrameric complexes. Simultaneously, we access information on the internal molecular mobility of ovalbumin on the nanometer length scale and compare it with results obtained for bovine serum albumin, immunoglobulin, and  $\beta$ -lactoglobulin.



## 1. INTRODUCTION

Protein assemblies such as clusters in liquid solutions are of fundamental interest regarding biological self-organization.<sup>1–3</sup> It is often difficult to understand such assemblies by solely employing static methods such as small-angle scattering, and experiments probing the protein dynamics are therefore performed in addition.<sup>4–8</sup> This observation holds in particular when protein assemblies are not static but dynamic or transient.<sup>9</sup>

Self-assembled protein aggregates can be reasons for diseases such as eye cataract,<sup>10</sup> sickle cell anemia,<sup>11</sup> Alzheimer's disease, and Parkinson's disease<sup>12</sup> but are also interesting for medical applications.

In this context, incoherent quasielastic neutron scattering (QENS) allows to unambiguously access the self-diffusion of particles with nanometer hydrodynamic radii suspended in aqueous solutions. Using deuterated solvents, neutron backscattering spectroscopy becomes predominantly sensitive to the prevailing incoherent scattering from the protein tracer particles.<sup>13</sup> Systematic studies of the diffusive dynamics of protein solutions permit to address the effect of macromolecular crowding<sup>14,15</sup> on both the global and internal motions of proteins.<sup>16–18</sup> It has been shown that these two contributions can be reliably separated using high-resolution QENS.<sup>13,17–19</sup> Moreover, it has been shown that the translational center-of-mass diffusion of globular proteins as a function of the protein concentration in the solution can be

quantitatively described in terms of the diffusion of colloidal hard spheres.<sup>17</sup> Besides macromolecular crowding, the diffusive dynamics depends also on control parameters such as the sample temperature<sup>20,21</sup> and the charge state influenced by the possible presence of salt ions in the solution.<sup>19,22</sup> Changes in the diffusive behavior because of structural changes induced by denaturation<sup>20,23</sup> or by mutations<sup>24</sup> could also be investigated. These studies on simplified model systems composed of a single target protein in water complement other neutron spectroscopy studies on more complex systems which mimic in vivo conditions, including the diffusion of selectively labeled proteins in deuterated living cells.<sup>25</sup> By comparing spectra collected with deuterated and hydrogenated solvents, it is also possible to determine the dynamics of the solvent in vivo.<sup>26,27</sup>

Ultimately, the aggregation of proteins from a monomeric suspension into clusters caused by the presence of multivalent salt ions has been explored using high-resolution incoherent neutron spectroscopy<sup>19,28</sup> and can be interpreted in terms of the theory of so-called patchy colloidal particles.<sup>29,30</sup> This agreement points to the future perspective of quantitatively understanding and controlling dynamic processes governing the formation of protein clusters and larger protein aggregates.

Received: May 7, 2018

Revised: August 14, 2018

Published: August 14, 2018

A very useful observation made in several previous studies on the diffusion of model proteins in aqueous solutions is that the protein center-of-mass undergoes a strictly Brownian diffusion on the nanosecond and nanometer observation scales of QENS and even in “physiologically” crowded suspensions (i.e., at volume fractions of up to approximately 30%).<sup>13,17–19,31,32</sup> Importantly, this observation is made without imposing it as an assumption in the model fitting, implying that the dependencies of the different contributions from the global and internal motions of proteins are obtained independently from the same data set. The Brownian character of the center-of-mass diffusion has in particular been further corroborated on backscattering spectrometers with an intermediate resolution and broader energy-transfer range. Because of the increasingly broad spectral contribution of the center-of-mass diffusion from dilute suspensions at high scattering vectors  $q$ , these spectrometers best access the high- $q$  range.<sup>13,19</sup>

The observed Brownian center-of-mass diffusion strictly obeys a Stokes–Einstein temperature dependence<sup>20</sup> and, importantly, as already indicated above, a dependence on the protein volume fraction in the solution that follows the model for the short-time diffusive properties of colloidal hard-sphere suspensions.<sup>17</sup> Given this previous observation, it is now possible to conversely infer the size of a macromolecular assembly such as a protein cluster via its effective hydrodynamic radius which defines its Brownian center-of-mass diffusion.<sup>28</sup> In this way, a possible dependence of the formation of protein assemblies on external parameters such as the protein concentration can be explored. Moreover, the observation timescale of the employed spectrometer, given by the energy resolution of the instrument, provides information on the lifetime of such an assembly.

In addition to the information on the center-of-mass motion of the assemblies, the elastic incoherent structure factor<sup>33</sup> (EISF) and a characteristic linewidth associated with the internal molecular fluctuations, that can be compared between different proteins, are obtained.

Here, we present a high-resolution neutron backscattering study of ovalbumin (OVA) protein suspensions in heavy water ( $D_2O$ ). We investigate the oligomerization based on the results of the global diffusion and we compare the internal dynamics to bovine serum albumin (BSA), immunoglobulin (Ig), and  $\beta$ -lactoglobulin (BLG) protein solutions. The global diffusion of BSA, Ig, and BLG was investigated by Grimaldo et al. in 2015<sup>20</sup> and 2014<sup>18</sup> and by Braun et al.,<sup>28</sup> respectively. OVA is an approximately globular protein, and aqueous OVA solutions have been studied previously using small-angle scattering.<sup>34</sup> Its structure has been understood in terms of tetrameric assemblies that constitute the basic building blocks of OVA crystals studied in protein crystallographic experiments. In liquid solutions, it appears that the OVA tetramer may dissociate into dimers and monomers. However, this possible dissociation has been subject to debate because small-angle X-ray scattering (SAXS) measurements and other physicochemical measurements such as analytical ultracentrifugation resulted in conflicting results.<sup>35</sup> Our results using QENS suggest that the dissociation of OVA tetramers may occur at sufficiently low protein concentrations.

## 2. EXPERIMENTS AND METHODS

Chicken egg-white OVA (A5503,  $\geq 98\%$  purity), BSA (A3059,  $\geq 98\%$  purity), the polyclonal Ig bovine  $\gamma$ -globulin Ig (G5009

$\geq 99\%$  purity), and BLG (L3908,  $\geq 90\%$  purity) were obtained as lyophilized powders from Sigma-Aldrich and used without further purification.

Solutions were prepared by a direct dissolution of the mass  $m_p$  of protein powder in the volume  $V$  of  $D_2O$ , defining the observable nominal protein concentration  $c_p = m_p/V$ . The resulting dry protein volume fraction in the solution is calculated as<sup>17</sup>

$$\varphi = \frac{m_p \nu_p}{V + m_p \nu_p} \quad (1)$$

where  $\nu_p = 0.746$  mL/g is the specific volume of OVA at 25 °C.<sup>36–38</sup>

The dry volume fraction  $\varphi$  from eq 1 can be linked to the real protein concentration  $c_{p,\text{real}} = \varphi/\nu_p$ .

The experimental data were recorded on the neutron backscattering spectrometer IN16B at the Institut Max von Laue—Paul Langevin, Grenoble, France,<sup>39</sup> using Si(111) monochromator and analyzer crystals, setting the elastic wavelength to 6.27 Å. A phase space transformer<sup>40</sup> was used to optimize the neutron flux at the sample position. The energy resolution function  $\mathcal{R}(\omega)$  had an approximative width of  $\approx 0.9$   $\mu\text{eV}$  full width half-maximum and was described analytically by a fit of two Gaussian functions to the measured spectrum from a vanadium sample.<sup>13</sup> The spectrometer chamber was kept in vacuum during the acquisition. The samples were filled into cylindrical, indium-sealed aluminium sample holders and held in a standard orange cryofurnace during the data acquisition. In total, 18 detectors were used to cover a scattering vector  $q$ -range of approximately  $0.2 \text{ \AA}^{-1} \leq q \leq 1.9 \text{ \AA}^{-1}$ .

The data reduction and analysis followed previously published protocols.<sup>13,18</sup> The employed model for the scattering function  $S$  depending on the scattering vector  $q$  and energy transfer  $\hbar\omega$  was

$$S(q, \omega) = \mathcal{R} \otimes \{ \beta(q) [A_0(q) \mathcal{L}(\gamma(q), \omega) + (1 - A_0(q)) \mathcal{L}(\gamma(q) + \Gamma(q), \omega)] + \beta_{D_2O}(q) \mathcal{L}(\gamma_{D_2O}(q), \omega) \} \quad (2)$$

Therein,  $\mathcal{R} = \mathcal{R}(q, \omega)$  denotes the spectrometer resolution function,  $\mathcal{L}(\gamma, \omega)$  represents a Lorentzian function with the width  $\gamma$ ,  $\beta(q)$  is an intensity scaling factor, and  $A_0(q)$  the EISF of the proteins. Importantly, in the present study, two types of fits using this model, eq 2, were carried out: (a) individual fits of the spectra for the different  $q$ -values ( $q < 1.8 \text{ \AA}^{-1}$ ) separately and (b) fits of the spectra for all  $q$ -values simultaneously,<sup>20</sup> denoted global fits. In the second case (b), the dependencies  $\gamma(q) = Dq^2$  and<sup>41</sup>

$$\Gamma(q) = \frac{D_{\text{int}} q^2}{1 + D_{\text{int}} q^2 \tau} \quad (3)$$

were imposed. Thus, the global diffusion associated with  $\gamma(q)$  was assumed to be Brownian, and the internal diffusion of the proteins associated with  $\Gamma(q)$  was assumed to obey a so-called jump diffusion<sup>41</sup> with the internal diffusion coefficient  $D_{\text{int}}$  and the residence time  $\tau$ . In contrast, the first approach (a) confirmed the validity within the errors of imposing  $\gamma = Dq^2$  and the jump diffusion determining  $\Gamma(q)$ , eq 3, in accordance with earlier studies.<sup>13,17–19</sup>

Example data and fits using eq 2 are depicted in Figure 1. In the plot, dash-dotted and dotted lines represent the result from

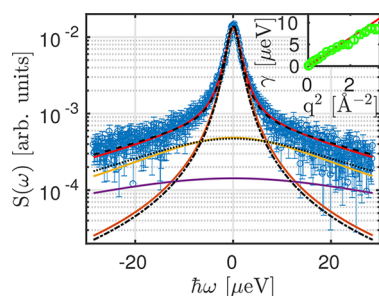


**Figure 1.** Example spectrum of OVA ( $c_p = 200$  mg/mL) in water ( $D_2O$ ) (symbols) recorded on IN16B at  $T = 295$  K and  $q = 0.56 \text{ \AA}^{-1}$ . The solid lines denote the results from the fit of the individual spectrum according to eq 2 without imposing any  $q$ -dependence. The red solid line superimposed on the symbols denotes the fit result composed of the Lorentzian with the width  $\gamma$  modeling the global diffusion (narrow brown line); the broader Lorentzian with the width  $\Gamma$  for internal dynamics (yellow line); and the nearly flat fixed water contribution (lower violet line). The dashed and dash-dotted lines superimposed on the solid lines depict the fit result and fit components in the case of the fit approach that imposes Brownian diffusion for the global motion and jump diffusion for the internal motion (see text). The water contribution is handled in the same way for both approaches. The inset shows  $\gamma$  versus  $q^2$  from the  $q$ -dependent fit (symbols). The solid line in the inset reports a fit of  $\gamma(q) = Dq^2$ .

the simultaneous fit of the spectra for all  $q$  at once, and solid lines report the result from the fits without imposing any  $q$ -dependence. We observe a good agreement of these two different fit approaches. The inset of Figure 1 displays the obtained  $\gamma(q)$  for the case of the individual fits for each  $q$  (symbols). This inset illustrates that the center-of-mass diffusion for the OVA solutions follows Brownian dynamics without imposing it. The small deviation of the fit results from  $\gamma(q) = Dq^2$  at the highest  $q$ -values is presumably because of cross-talking of the signals from the Lorentzian contributions with the widths  $\Gamma$  and  $\gamma$ .

The EISF  $A_0(q)$  resulting from the fit of eq 2 was fitted by<sup>18,33,42</sup>

$$A_0(q) = p_0 + (1 - p_0)[p_1 A_{3\text{-jump}}(q) + (1 - p_1) A_{\text{sphere}}(q)] \quad (4)$$

Therein,  $p_0$  denotes the fraction of hydrogen atoms that appear immobile on the observation timescale of our experiment.  $p_1$  is the fraction of the mobile hydrogen atoms undergoing a jump diffusion between three sites. The

remaining hydrogen atoms  $(1 - p_0)(1 - p_1)$  are assumed to undergo a diffusion inside an impermeable sphere with the confinement radius  $R_s$ .  $A_{3\text{-jump}}(q)$  and  $A_{\text{sphere}}(q)$  are described as follows<sup>18,33,42</sup>

$$A_{3\text{-jump}}(q) = \frac{1}{3[1 + 2j_0(qa)]} \quad (5)$$

and

$$A_{\text{sphere}}(q) = \left| \frac{3j_1(qR_s)}{qR_s} \right|^2 \quad (6)$$

where  $j_0 = \sin(x)/x$  and  $j_1(x)$  denote the spherical Bessel functions of the zeroth and first order, respectively. The three-site jump diffusion, eq 5 is assumed to be due to the reorientation of methyl groups  $-\text{CH}_3$ , associated with a fixed jump distance  $a = 1.715 \text{ \AA}$ .<sup>18,33,42</sup>

All data reductions and fits were performed using MATLAB (The MathWorks, Inc.), partly involving MATLAB “mex”-files employing the GNU Scientific Libraries for numerical integration and root finding.<sup>13,17</sup>

### 3. THEORY AND MODELING

From the tetrameric crystal structure ( $N = 4$ ) of OVA (PDB 1OVA, four chains),<sup>43</sup> we have extracted a dimeric structure ( $N = 2$ ) by using only the closely bound chains A and B from the tetrameric structure. For the monomer structure ( $N = 1$ ), we used chain A.

For each of the three structures, HYDROPRO<sup>44</sup> was used to calculate the translational and rotational diffusion coefficients in the limit of infinite dilution,  $D_{t,0} = D_{t,0}(N)$  and  $D_{r,0} = D_{r,0}(N)$  as well as the radius of gyration  $R_g = R_g(N)$ , as summarized in Table 1.

The hydrodynamic radii  $R_h(N)$  were calculated from the translational diffusion coefficients  $D_{t,0}$  determined with HYDROPRO.

For consistency with the neutron data, the HYDROPRO calculations were performed using the viscosity and solution density of  $D_2O$ .<sup>45</sup>

Moreover, the GROMACS<sup>46</sup> tool *pdb2gmx* was used to add the missing hydrogen atoms. Mathematica was used to extract the positions of the hydrogen atoms in these protein monomer, dimer, and tetramer structures. From the thus obtained hydrogen coordinates, the radial hydrogen density distribution functions  $\rho(r, N)$  for these three structures were calculated (Figure 2).

**Table 1.** Table of Properties of OVA Monomers, Dimers, and Tetramers Calculated Using HYDROPRO<sup>44</sup> for  $D_2O$  Solutions (See Text)<sup>a</sup>

	$N$	$R_g$ [nm]	$R_h$ [nm]	$T$ [K]	$D_{t,0}$ [ $\text{\AA}^2/\text{ns}$ ]	$D_{r,0}$ [1/ns]	$D_0$ [ $\text{\AA}^2/\text{ns}$ ]
monomer	1	2.28	2.8749	280	3.82	0.00341	4.74
				295	6.30	0.00562	7.80
				310	9.39	0.00838	11.60
dimer	2	2.83	3.6029	280	3.05	0.00168	3.82
				295	5.02	0.00277	6.30
				310	7.49	0.00413	9.40
tetramer	4	3.53	4.5944	280	2.39	0.000838	3.00
				295	3.94	0.00138	4.94
				310	5.88	0.00206	7.37

<sup>a</sup>The hydrodynamic radii  $R_h$  are calculated from the translational diffusion coefficients in the dilute limit  $D_{t,0}$ .  $D_0$  is the apparent diffusion coefficient in the dilute limit calculated by eq 9 with  $D_t = D_{t,0}$  and  $D_r = D_{r,0}$ .  $R_g$  is the radius of gyration.

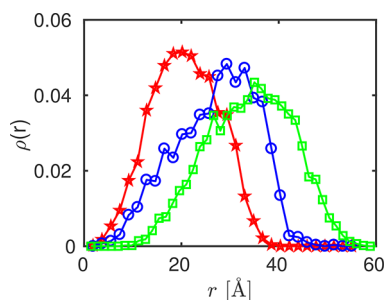


**Figure 2.** Radial hydrogen density distribution functions  $\rho(r, N)$  of the OVA monomer (star symbols), dimer (circles), and tetramer (squares), obtained from the associated protein data bank (PDB) structure files as described in the text.

The diffusion coefficients depend on the effective volume fraction

$$\phi = \varphi \cdot (R_h/R)^3 \quad (7)$$

with the effective sphere radius  $R$  calculated from the specific volume  $\nu_p$  and the molar mass  $M_w$ <sup>17,18,47,48</sup>

$$R = \sqrt[3]{\frac{3 \nu_p M_w}{4\pi N_A}} \quad (8)$$

with the Avogadro constant  $N_A$  and the molecular weight of a monomer  $M_w = 42.7$  kDa.<sup>49</sup>

By rescaling the volume fraction using an effective radius, anisotropy effects and influences due to the hydration layer are taken into account.<sup>17</sup>

Established analytical expressions for hard spheres for  $f_t(\phi)$  (ref 50 eqs 11 and 12) and  $f_r(\phi)$  (ref 51 eq 21) were used to rescale the translational and rotational diffusion coefficients, respectively, for the different protein oligomers, that is,  $D_t(\phi) = D_{t0}f_t(\phi)$  and  $D_r(\phi) = D_{r0}f_r(\phi)$  which were then used to calculate the volume fraction dependent apparent diffusion coefficient.

The apparent diffusion coefficient  $D$  can be obtained from the solution of the implicit equation<sup>13,17</sup>

$$\sum_{l=0}^n B_l(q) \frac{D_t l(l+1) + (D_t - D)q^2}{[D_t l(l+1) + (D_t + D)q^2]^2} = 0 \quad (9)$$

where  $n$  has to be chosen large enough to obtain convergence on the desired  $q$ -range.<sup>13</sup> For our case, we chose  $n = 75$ .

$B_l(q)$  in eq 9 is determined by the radial distribution of hydrogens  $\rho(r, N)$  via

$$B_l(q) = (2l+1) \int_0^\infty dr \rho(r, N) j_l^2(qr) \quad (10)$$

with the  $l$ th order spherical Bessel functions of first kind,  $j_l(x)$ .

The values for  $D$  from HYDROPRO for the monomer are consistent with published results for native OVA obtained using dynamic light scattering in H<sub>2</sub>O solutions, namely,  $D_0 = 8.7$  Å<sup>2</sup>/ns at  $T = 25$  °C<sup>52</sup> and  $D_0 = 7.1$  Å<sup>2</sup>/ns at  $T = 20$  °C.<sup>53</sup>

## 4. RESULTS AND DISCUSSION

**4.1. Rotational and Translational Diffusion.** The observable apparent diffusion coefficients  $D$  of OVA given by  $\gamma(q) = Dq^2$  with the fitted  $\gamma$  according to eq 2 are depicted in Figure 3. The experimental values of  $D$  are depicted for the two distinct fit approaches explained in the **Experiment and Methods** section: (a) by a fit without a priori imposing  $\gamma(q) =$

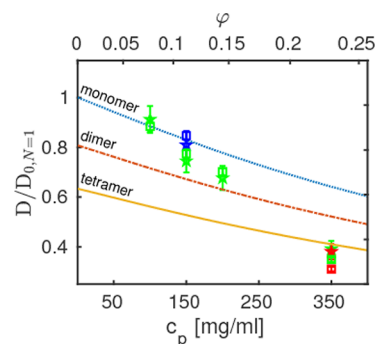


**Figure 3.** Normalized apparent diffusion coefficients of OVA (symbols) obtained from the fits. Square symbols denote results obtained from a global fit imposing the  $q$ -dependence of the global apparent diffusion  $\gamma(q) = Dq^2$  and jump diffusion for the internal dynamics. Star symbols denote results obtained by fitting  $\gamma(q) = Dq^2$  to the fit results for  $\gamma(q)$ . The samples were measured at the temperatures  $T = 280, 295,$  and  $310$  K (blue, red, and green symbols, respectively). The lower  $x$ -axis denotes the nominal protein concentrations  $c_p$  (equation 1) from the sample preparation, that is, the weighed dry protein powder mass per volume of D<sub>2</sub>O that it was dissolved in, and the upper  $x$ -axis represents the calculated dry protein volume fraction  $\varphi$  (equation 1). The lines indicate the theoretical apparent diffusion coefficients for OVA monomers (dotted), dimers (dash-dotted), and tetramers (solid), respectively, calculated using eq 9.

$Dq^2$  (star symbols) and (b) by a global fit imposing  $\gamma(q) = Dq^2$  and  $\Gamma(q) = D_{int}q^2/(1 + D_{int}q^2\tau)$  (square symbols, cf. **Experiments and Methods**). The results for both approaches agree very well.

The observed apparent diffusion coefficients scale with the temperature and protein concentration as expected, that is, the diffusion increases with rising temperature and decreases with rising protein concentration. For a better readability of the plot, the diffusion coefficients are normalized by the monomer diffusion coefficient in the dilute limit at the given temperature.

Figure 3 also reports an interpretation of these results for  $D$  by plotting the calculated apparent diffusion coefficients  $D(\phi) = f(D_t(\phi), D_r(\phi))$  using eq 9 for OVA monomers (dash-dotted), dimers (dotted), and tetramers (solid) based on colloid models for the short-time self-diffusion of hard spheres. This calculation is based on eqs 7 and 9 with the assumptions for  $D_t = D_t(\phi, N)$ ,  $D_r = D_r(\phi, N)$  and  $\rho(r, N)$  (Figure 2) as explained in the **Theory and Modeling** section. The samples are prepared with the nominal concentration  $c_p$  of the proteins in D<sub>2</sub>O (lower  $x$ -axis in Figure 3), resulting in the dry protein volume fraction  $\varphi$  using eq 1 (upper  $x$ -axis in Figure 3).

By comparing the experimental observation and theory, our results indicate that at  $T = 295$  K OVA assemblies are, on average, nearly monomeric at  $c_p = 100$  mg/mL, approximately dimeric at 200 mg/mL, and tetrameric at  $c_p = 350$  mg/mL. The distribution may depend slightly on temperature as suggested by the slight spread of the symbols for  $c_p = 150$  mg/mL. We assume that a distribution of  $N$ -mers is present that increasingly shifts to a tetrameric assembly with rising protein volume fraction. Here, we emphasize that in the present picture, the oligomers are seen as rigid assemblies in our experiment with an observation time on the order of 1 ns.

The oligomers may be subject to internal fluctuations of the monomeric building blocks relative to each other, or be subject to a dissociation of these building blocks, on longer timescales. Moreover, a distribution of  $N$ -mers with different  $N$  may result

in an average apparent  $N$  because of the limited accuracy and ensemble-averaging in our experiment.

**4.2. Internal Diffusion.** Simultaneously with the fit results for  $D$ , we obtain results on the internal molecular nanosecond relaxation motion of OVA in  $D_2O$ . Our experiment observes these internal diffusive motions on a nanometer length scale, and, thus, displacements smaller than the protein radius. For the internal diffusion, we employ the individual fit approach for the spectra at each  $q$  separately, because the jump diffusion model, eq 3, only constitutes an approximate model of the internal diffusion. This model has nevertheless been shown to be sufficiently suitable for proteins at physiological temperatures.<sup>18,20,54</sup> We obtain  $\Gamma(q)$  and  $A_0(q)$  (eq 2) from this fit. Figure 4 depicts the resulting EISF  $A_0(q)$  associated with the

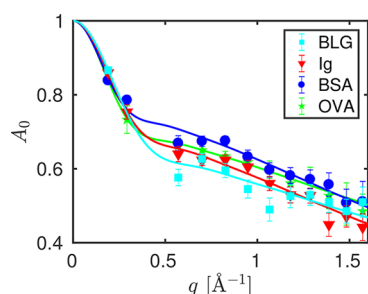


**Figure 4.** Fit results (symbols) from eq 2 for the EISF  $A_0(q)$  at  $T = 295$  K and  $c_p = 200$  mg/mL (Ig, BSA, OVA) and  $c_p = 300$  mg/mL (BLG), and fit of eq 4 to these results (lines). Square symbols denote BLG, triangle symbols denote Ig, circle symbols denote BSA, and star symbols denote OVA.

internal diffusive motions of the proteins and the fits of eq 4. The resulting fit parameters for the EISF are given in Table 2. The EISF from the different proteins are nearly indistinguishable within the limits of the present experimental accuracy, as well as independent from the crowding. The latter observation is consistent with earlier findings.<sup>18</sup> The value for BSA is in good agreement with the value found at  $T = 295$  K in an earlier study using a different neutron spectrometer.<sup>20</sup>

The confinement radius  $R_s$  does appear to have a systematic dependence on the protein size. We note, however, that the fit results for  $R_s$  sensitively depend on  $A_0(q)$  at the lowest values for  $q$  which are measured with the lowest two detectors. For these two detectors, we may have systematic errors because the overall linewidth is small and thus approaches the resolution. Therefore, the results depend sensitively on the model of the resolution function. In addition, the intensity at low  $q$  might be affected by coherent scattering.

The values for the linewidth  $\Gamma(q)$  associated with the internal dynamics are shown in Figure 5 for exemplary data sets. We subsequently fit eq 3 to  $\Gamma(q)$ . The resulting fit parameters  $D_{\text{int}}$  and  $\tau$  for all data sets are summarized in Figure

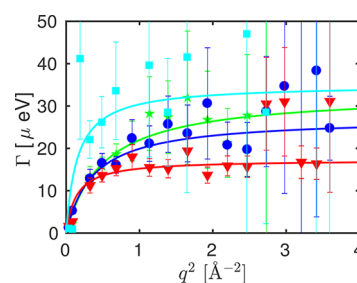


**Figure 5.** Fit results for the linewidth of the Lorentzian contribution  $\Gamma(q)$  associated with the internal molecular mobility of the proteins at  $T = 295$  K and  $c_p = 200$  mg/mL as a function of the scattering vector  $q$  (eq 2), and fit of eq 3 ( $0.4 \text{ \AA}^{-2} < q^2 < 3.3 \text{ \AA}^{-2}$ ) to these results (lines). Square symbols denote BLG, triangle symbols denote Ig, circle symbols denote BSA, and star symbols denote OVA.

6 for different proteins with different concentrations measured at  $T = 295$  K.

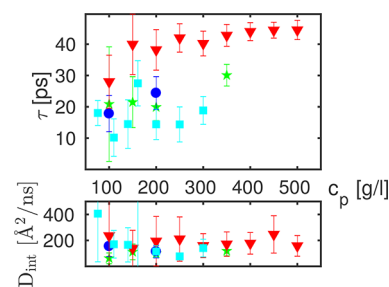


**Figure 6.** Top: Residence times at  $T = 295$  K associated with the internal protein motions as a function of the protein concentration  $c_p$  obtained from a fit of eq 3 to the widths  $\Gamma(q)$  (see Figure 5) based on  $q$ -dependent fits. Square symbols denote BLG, triangle symbols denote Ig, circle symbols denote BSA, and star symbols denote OVA. Bottom: Internal diffusion coefficients obtained from the same fits.

Overall, the present results show that different proteins are characterized by remarkably distinct internal fluctuations. We have therefore looked for systematic correlations with properties of the proteins, namely, the percentage of  $\beta$ -sheets or helices in the secondary structure of the protein, the protein surface, and surface-to-volume ratio, as determined with the 3V software,<sup>55</sup> by using the PDB structures 1OVA chain A,<sup>43</sup> 3V03,<sup>56</sup> 1IGT,<sup>57</sup> and 4Y0P<sup>58</sup> for OVA, BSA, Ig, and BLG, respectively. The corresponding values are also displayed in Table 2.

We have not found a parameter that would link the results for all four investigated proteins in a monotonous way (see Figure S2), that is, no obvious correlations were found.

**4.3. Limitations of the Current Analysis and Interpretation.** We stress that all analyses presented in this work are subject to assumptions and modeling, and the

**Table 2.** Fit Parameters for the EISF in Figure 4 and Protein Properties Calculated with the 3V Software<sup>55</sup> (Surface and Volume) and Percentage of Amino-Acids in Helical Structure and in  $\beta$ -Sheet Obtained From the PDB

	$R_s$ [Å]	$p_0$	$p_1$	surface [nm <sup>2</sup> ]	volume [nm <sup>3</sup> ]	% of helix	% of $\beta$ -sheet
OVA	9.87 ± 0.40	0.35 ± 0.04	0.54 ± 0.05	109.10	58.621	32	32
BSA	10.88 ± 1.86	0.30 ± 0.11	0.65 ± 0.11	357.77	180.032	74	0
Ig	8.84 ± 0.89	0.27 ± 0.08	0.59 ± 0.08	450.50	205.833	6	49
BLG	7.79 ± 0.90	0.35 ± 0.11	0.45 ± 0.16	58.95	24.996	16	40

interpretation of the results is subject to the validity of these assumptions, which we tentatively summarize here.

Regarding the analysis of the rotational and translational diffusion (subsection 4.1), we have used a colloidal hard-sphere model. In this context, the following issues have to be noted:

First, the excluded volume fraction  $\varphi$  by the proteins is calculated based on an effective sphere volume of compact clusters. In the case of less compact clusters, this assumption might not hold anymore, and a larger effective  $\varphi$  would be expected. Second, the theoretical  $\varphi$ -dependence of the diffusion of the oligomers is calculated based on the assumption of noncharged colloidal spheres.<sup>50,51</sup> The validity of this approximation might break down in case of a strong interaction between the clusters, as well as for strongly non-spherical clusters. In fact, for attractive systems, a decay of  $D$  as a function of  $\varphi$  faster than expected for uncharged hard spheres has been observed.<sup>15</sup> Third, since our QENS experiment accesses an ensemble-average, the clusters may be subject to a size distribution with unknown dispersity, but an average size that increases with  $\varphi$  (as previously observed in lysozyme solutions<sup>7</sup>).

For a full picture regarding the cluster formation, both comprehensive SAXS data and neutron spin-echo data recorded under the same sample conditions (i.e., at the same protein concentrations in D<sub>2</sub>O solutions without additional buffers) would be required in addition to our neutron backscattering data,<sup>28</sup> ideally employing protein samples from the same production batch. In the absence of such comprehensive data, our interpretation of cluster formation may remain ambiguous.

Regarding the internal molecular diffusive motions we note that the possibility to observe the internal motions on IN16B is presently limited by the explored maximum energy range  $\hbar\omega \leq 30 \mu\text{eV}$ . Moreover, the jump diffusion model, eq 3, for the internal diffusion obviously constitutes an approximation of more complex motions.<sup>16,20,54</sup> More fundamentally, even the Lorentzian  $\Gamma(q)$  in eq 2 accounting for the internal motions in the fit constitutes an approximation only of a more complex scattering function. There is no strong physical but only a heuristic justification of the jump diffusion model because it reproduces the observed  $q$ -dependence of  $\Gamma(q)$  quite well. Nevertheless, the residence time  $\tau$  showing the main differences could also be extracted by taking an average of the asymptotic values at high  $q$  values. Furthermore, the energy landscape of a protein contains many local minima which the hydrogens have to overcome to get to a new position. It is therefore reasonable to assume that the atoms stay at one position during the residence time  $\tau$  before performing a diffusive jump. For this reason, the jump diffusion model appears justified to some level. To identify the driving parameters leading to distinct dynamics in different proteins, backscattering spectrometers having a broader energy range but broader energy resolution may be employed in addition in further studies.<sup>20,59,60</sup> Moreover, the internal motions may in the future be further investigated by molecular dynamics simulations. A scattering function calculated from such simulation results would then replace  $\Gamma(q)$  in the fits.

## 5. CONCLUSIONS

The ensemble-averaged short-time protein center-of-mass self-diffusion in aqueous (D<sub>2</sub>O) OVA solutions observed using neutron backscattering spectroscopy is not consistent with the

picture of rigidly bound OVA tetramers over the entire range of protein concentrations explored. In contrast, both OVA monomers and dimers may be present at low concentration. The results for the nominal protein concentrations of 100 and 150 mg/mL point to a suspension consisting predominantly of monomers and dimers, and solely of dimers at 200 mg/mL. At 350 mg/mL, tetramers or even larger aggregates appear to prevail. However, the aggregation state of OVA may depend sensitively on various environmental parameters and even the specific protein batch explored. We also point out that our aqueous sample solutions were based on D<sub>2</sub>O without any buffer, and results can differ if H<sub>2</sub>O<sup>61,62</sup> or if an additional buffer is used. Moreover, we used an effective hard-sphere model to rescale the diffusion coefficients, obtained from the pdb structures in the dilute limit, to the desired volume fraction.

Our results illustrate the general possibility and describe the methodological framework, using QENS, to infer on the assembly size and in this way, more generally, on solution structure properties. Because the scattering signal from the proteins in our samples is mainly incoherent, we unambiguously detect the self-diffusion or, synonymously, tracer diffusion of the protein  $N$ -mers, clusters, or aggregates independent from their size. Moreover, another advantage of incoherent QENS over complementary scattering methods consists in the linear dependence of the scattering signal on the size of the assemblies, aggregates, or clusters, that is, the possible presence of large aggregates at a comparatively small partial number density in a dispersed suspension would not “cover up” the scattering signal from any possibly prevailing monomers.

We emphasize that our current work addresses and illustrates the methodology of neutron backscattering data analysis, and our resulting picture of the cluster formation in the OVA protein solution system is based on the observed global diffusion. For a complete picture, a combination of other experimental techniques including small-angle scattering and neutron spin-echo spectroscopy is required in addition to neutron backscattering,<sup>28</sup> ideally complemented by simulations. Without such complementary information, ambiguities may remain regarding the interpretation of the results.

We simultaneously obtain information on the internal molecular mobility of the investigated proteins. By comparing those of OVA with the other model proteins BLG, BSA, and Ig, we observe clear differences, which do not correlate in an obvious manner with the structural properties of the protein such as the percentage of  $\beta$ -sheet or helices or the surface-to-volume ratio. Further studies will be needed to better understand how internal motions on the sub-nanosecond timescale are tuned in different proteins.

## ■ ASSOCIATED CONTENT

### 📄 Supporting Information

The Supporting Information is available free of charge on the ACS Publications website at DOI: 10.1021/acs.jpcc.8b04349.

The neutron data are permanently curated by the ILL and accessible via <http://dx.doi.org/10.5291/ILL-DATA.9-13-477> (OVA, Ig, and BSA), and <http://dx.doi.org/10.5291/ILL-DATA.8-04-724> (BLG). Diffusion coefficients calculated for spheres with equivalent hydrodynamic radii compared with the ones calculated for the different clusters and the averaged residence

times as a function of the radii of gyration for different proteins (PDF)

## AUTHOR INFORMATION

### Corresponding Author

\*E-mail: seydel@ill.eu.

### ORCID

Christian Beck: 0000-0001-7214-3447

Felix Roosen-Runge: 0000-0001-5106-4360

Michal K. Braun: 0000-0002-9642-7492

Fajun Zhang: 0000-0001-7639-8594

Tilo Seydel: 0000-0001-9630-1630

### Notes

The authors declare no competing financial interest.

## ACKNOWLEDGMENTS

This work was supported in part by the DFG and the ANR (contract no. ANR-16-CE92-0009-01) and the Knut and Alice Wallenberg Foundation (project grant KAW 2014.0052). C.B. acknowledges the support by a studentship co-funded by the ILL and the University of Tübingen. We thank R. Ammer (ILL) for help during the IN16B experiment.

## REFERENCES

- (1) Dinsmore, A. D.; Dubin, P. L.; Grason, G. M. Clustering in Complex Fluids. *J. Phys. Chem. B* **2011**, *115*, 7173–7174.
- (2) Johnston, K. P.; Maynard, J. A.; Truskett, T. M.; Borwankar, A. U.; Miller, M. A.; Wilson, B. K.; Dinin, A. K.; Khan, T. A.; Kaczorowski, K. J. Concentrated Dispersions of Equilibrium Protein Nanoclusters That Reversibly Dissociate into Active Monomers. *ACS Nano* **2012**, *6*, 1357–1369.
- (3) Yearley, E. J.; Godfrin, P. D.; Perevozchikova, T.; Zhang, H.; Falus, P.; Porcar, L.; Nagao, M.; Curtis, J. E.; Gawande, P.; Taing, R.; et al. Observation of Small Cluster Formation in Concentrated Monoclonal Antibody Solutions and Its Implications to Solution Viscosity. *Biophys. J.* **2014**, *106*, 1763–1770.
- (4) Stradner, A.; Sedgwick, H.; Cardinaux, F.; Poon, W. C. K.; Egelhaaf, S. U.; Schurtenberger, P. Equilibrium Cluster Formation in Concentrated Protein Solutions and Colloids. *Nature* **2004**, *432*, 492–495.
- (5) Porcar, L.; Falus, P.; Chen, W.-R.; Faraone, A.; Fratini, E.; Hong, K.; Baglioni, P.; Liu, Y. Formation of the Dynamic Clusters in Concentrated Lysozyme Protein Solutions. *J. Phys. Chem. Lett.* **2010**, *1*, 126–129.
- (6) Liu, Y.; Porcar, L.; Chen, J.; Chen, W.-R.; Falus, P.; Faraone, A.; Fratini, E.; Hong, K.; Baglioni, P. Lysozyme Protein Solution with an Intermediate Range Order Structure. *J. Phys. Chem. B* **2011**, *115*, 7238–7247.
- (7) Cardinaux, F.; Zaccarelli, E.; Stradner, A.; Bucciarelli, S.; Farago, B.; Egelhaaf, S. U.; Sciortino, F.; Schurtenberger, P. Cluster-Driven Dynamical Arrest in Concentrated Lysozyme Solutions. *J. Phys. Chem. B* **2011**, *115*, 7227–7237.
- (8) Okumura, H.; Higashi, M.; Yoshida, Y.; Sato, H.; Akiyama, R. Theoretical Approaches for Dynamical Ordering of Biomolecular Systems. *Biochim. Biophys. Acta, Gen. Subj.* **2018**, *1862*, 212–228.
- (9) Nawrocki, G.; Wang, P.-h.; Yu, L.; Sugita, Y.; Feig, M. Slow-Down in Diffusion in Crowded Protein Solutions Correlates with Transient Cluster Formation. *J. Phys. Chem. B* **2017**, *121*, 11072–11084.
- (10) Benedek, G. B. Cataract as a Protein Condensation Disease: The Proctor Lecture. *Invest. Ophthalmol. Visual Sci.* **1997**, *38*, 1911–1921.
- (11) Galkin, O.; Chen, K.; Nagel, R. L.; Hirsch, R. E.; Vekilov, P. G. Liquid-liquid separation in solutions of normal and sickle cell hemoglobin. *Proc. Natl. Acad. Sci. U.S.A.* **2002**, *99*, 8479–8483.
- (12) Ross, C. A.; Poirier, M. A. Protein Aggregation and Neurodegenerative Disease. *Nat. Med.* **2004**, *10*, S10–S17.
- (13) Grimaldo, M.; Roosen-Runge, F.; Jalarvo, N.; Zamponi, M.; Zanini, F.; Hennig, M.; Zhang, F.; Schreiber, F.; Seydel, T. High-Resolution Neutron Spectroscopy on Protein Solution Samples. *EPJ Web Conf.* **2015**, *83*, 02005.
- (14) Ellis, R. J. Macromolecular Crowding: An Important but Neglected Aspect of the Intracellular Environment. *Curr. Opin. Struct. Biol.* **2001**, *11*, 114–119.
- (15) Bucciarelli, S.; Myung, J. S.; Farago, B.; Das, S.; Vliegthart, G. A.; Holderer, O.; Winkler, R. G.; Schurtenberger, P.; Gompper, G.; Stradner, A. Dramatic Influence of Patchy Attractions on Short-Time Protein Diffusion under Crowded Conditions. *Sci. Adv.* **2016**, *2*, No. e1601432.
- (16) Monkenbusch, M.; Stadler, A.; Biehl, R.; Ollivier, J.; Zamponi, M.; Richter, D. Fast Internal Dynamics in Alcohol Dehydrogenase. *J. Chem. Phys.* **2015**, *143*, 075101.
- (17) Roosen-Runge, F.; Hennig, M.; Zhang, F.; Jacobs, R. M. J.; Sztucki, M.; Schober, H.; Seydel, T.; Schreiber, F. Protein Self-Diffusion in Crowded Solutions. *Proc. Natl. Acad. Sci. U.S.A.* **2011**, *108*, 11815–11820.
- (18) Grimaldo, M.; Roosen-Runge, F.; Zhang, F.; Seydel, T.; Schreiber, F. Diffusion and Dynamics of  $\gamma$ -Globulin in Crowded Aqueous Solutions. *J. Phys. Chem. B* **2014**, *118*, 7203–7209.
- (19) Grimaldo, M.; Roosen-Runge, F.; Hennig, M.; Zanini, F.; Zhang, F.; Zamponi, M.; Jalarvo, N.; Schreiber, F.; Seydel, T. Salt-Induced Universal Slowing Down of the Short-Time Self-Diffusion of a Globular Protein in Aqueous Solution. *J. Phys. Chem. Lett.* **2015**, *6*, 2577–2582.
- (20) Grimaldo, M.; Roosen-Runge, F.; Hennig, M.; Zanini, F.; Zhang, F.; Jalarvo, N.; Zamponi, M.; Schreiber, F.; Seydel, T. Hierarchical Molecular Dynamics of Bovine Serum Albumin in Concentrated Aqueous Solution Below and Above Thermal Denaturation. *Phys. Chem. Chem. Phys.* **2015**, *17*, 4645–4655.
- (21) Hennig, M.; Roosen-Runge, F.; Zhang, F.; Zorn, S.; Skoda, M. W. A.; Jacobs, R. M. J.; Seydel, T.; Schreiber, F. Dynamics of Highly Concentrated Protein Solutions Around the Denaturing Transition. *Soft Matter* **2012**, *8*, 1628–1633.
- (22) Heinen, M.; Zanini, F.; Roosen-Runge, F.; Fedunová, D.; Zhang, F.; Hennig, M.; Seydel, T.; Schweins, R.; Sztucki, M.; Antalík, M.; et al. Viscosity and Diffusion: Crowding and Salt Effects in Protein Solutions. *Soft Matter* **2012**, *8*, 1404–1419.
- (23) Ameseder, F.; Radulescu, A.; Khanef, M.; Lohstroh, W.; Stadler, A. M. Homogeneous and Heterogeneous Dynamics in Native and Denatured Bovine Serum Albumin. *Phys. Chem. Chem. Phys.* **2018**, *20*, 5128–5139.
- (24) Stadler, A. M.; Garvey, C. J.; Embs, J. P.; Koza, M. M.; Unruh, T.; Artmann, G.; Zaccai, G. Picosecond Dynamics in Haemoglobin from Different Species: A Quasielastic Neutron Scattering Study. *Biochim. Biophys. Acta, Gen. Subj.* **2014**, *1840*, 2989–2999.
- (25) Anunciado, D. B.; Nyugen, V. P.; Hurst, G. B.; Doktycz, M. J.; Urban, V.; Langan, P.; Mamontov, E.; O'Neill, H. In Vivo Protein Dynamics on the Nanometer Length Scale and Nanosecond Time Scale. *J. Phys. Chem. Lett.* **2017**, *8*, 1899–1904.
- (26) Tehei, M.; Franzetti, B.; Wood, K.; Gabel, F.; Fabiani, E.; Jasnin, M.; Zamponi, M.; Oesterhelt, D.; Zaccai, G.; Ginzburg, M.; et al. Neutron Scattering Reveals Extremely Slow Cell Water in a Dead Sea Organism. *Proc. Natl. Acad. Sci. U.S.A.* **2007**, *104*, 766–771.
- (27) Stadler, A. M.; Embs, J. P.; Digel, I.; Artmann, G. M.; Unruh, T.; Büldt, G.; Zaccai, G. Cytoplasmic Water and Hydration Layer Dynamics in Human Red Blood Cells. *J. Am. Chem. Soc.* **2008**, *130*, 16852–16853.
- (28) Braun, M. K.; Grimaldo, M.; Roosen-Runge, F.; Hoffmann, I.; Czakkel, O.; Sztucki, M.; Zhang, F.; Schreiber, F.; Seydel, T. Crowding-Controlled Cluster Size in Concentrated Aqueous Protein Solutions: Structure, Self- and Collective Diffusion. *J. Phys. Chem. Lett.* **2017**, *8*, 2590–2596.
- (29) Matsarskaia, O.; Braun, M. K.; Roosen-Runge, F.; Wolf, M.; Zhang, F.; Roth, R.; Schreiber, F. Cation-Induced Hydration Effects

Cause Lower Critical Solution Temperature Behavior in Protein Solutions. *J. Phys. Chem. B* **2016**, *120*, 7731–7736.

(30) Roosen-Runge, F.; Zhang, F.; Schreiber, F.; Roth, R. Ion-activated Attractive Patches as a Mechanism for Controlled Protein Interactions. *Sci. Rep.* **2014**, *4*, 7016.

(31) Stadler, A. M.; van Eijck, L.; Demmel, F.; Artmann, G. Macromolecular Dynamics in Red Blood Cells Investigated Using Neutron Spectroscopy. *J. R. Soc., Interface* **2011**, *8*, 590–600.

(32) Doster, W.; Longeville, S. Microscopic Diffusion and Hydrodynamic Interactions of Hemoglobin in Red Blood Cells. *Biophys. J.* **2007**, *93*, 1360–1368.

(33) Bée, M. A physical insight into the elastic incoherent structure factor. *Phys. B* **1992**, *182*, 323–336.

(34) Ianeselli, L.; Zhang, F.; Skoda, M. W. A.; Jacobs, R. M. J.; Martin, R. A.; Callow, S.; Prévost, S.; Schreiber, F. Protein–Protein Interactions in Ovalbumin Solutions Studied by Small-Angle Scattering: Effect of Ionic Strength and the Chemical Nature of Cations. *J. Phys. Chem. B* **2010**, *114*, 3776–3783.

(35) Scott, D. J.; Patel, T. R.; Besong, D. M. T.; Stetefeld, J.; Winzor, D. J. Examination of the Discrepancy between Size Estimates for Ovalbumin from Small-Angle X-ray Scattering and Other Physicochemical Measurements. *J. Phys. Chem. B* **2011**, *115*, 10725–10729.

(36) Dayhoff, M. O.; Perlmann, G. E.; MacInnes, D. A. The Partial Specific Volumes, in Aqueous Solution, of Three Proteins. *J. Am. Chem. Soc.* **1952**, *74*, 2515–2517.

(37) Charlwood, P. A. Partial Specific Volumes of Proteins in Relation to Composition and Environment. *J. Am. Chem. Soc.* **1957**, *79*, 776–781.

(38) Zamyatnin, A. A. Protein Volume in Solution. *Prog. Biophys. Mol. Biol.* **1972**, *24*, 107–123.

(39) Frick, B.; Mamontov, E.; van Eijck, L.; Seydel, T. Recent Backscattering Instrument Developments at the ILL and SNS. *Z. Phys. Chem.* **2010**, *224*, 33–60.

(40) Hennig, M.; Frick, B.; Seydel, T. Optimum Velocity of a Phase-Space Transformer for Cold-Neutron Backscattering Spectroscopy. *J. Appl. Crystallogr.* **2011**, *44*, 467–472.

(41) Singwi, K. S.; Sjölander, A. Diffusive Motions in Water and Cold Neutron Scattering. *Phys. Rev.* **1960**, *119*, 863–871.

(42) Fitter, J. Confined Molecular Motions of Globular Proteins Studied in Powder Samples and in Solution. *J. Phys. IV* **2000**, *10*, Pr7-265–Pr7-270.

(43) Stein, P. E.; Leslie, A. G. W.; Finch, J. T.; Carrell, R. W. Crystal structure of uncleaved ovalbumin at 1.95 Å resolution. *J. Mol. Biol.* **1991**, *221*, 941–959.

(44) Ortega, A.; Amorós, D.; García de la Torre, J. Prediction of Hydrodynamic and Other Solution Properties of Rigid Proteins from Atomic- and Residue-Level Models. *Biophys. J.* **2011**, *101*, 892–898.

(45) Cho, C. H.; Urquidí, J.; Singh, S.; Robinson, G. W. Thermal Offset Viscosities of Liquid H<sub>2</sub>O, D<sub>2</sub>O, and T<sub>2</sub>O. *J. Phys. Chem. B* **1999**, *103*, 1991–1994.

(46) Berendsen, H. J. C.; van der Spoel, D.; van Drunen, R. GROMACS: A message-passing parallel molecular dynamics implementation. *Comput. Phys. Commun.* **1995**, *91*, 43–56.

(47) Svergun, D. I.; Richard, S.; Koch, M. H. J.; Sayers, Z.; Kuprin, S.; Zaccai, G. Protein Hydration in Solution: Experimental Observation by X-ray and Neutron Scattering. *Proc. Natl. Acad. Sci. U.S.A.* **1998**, *95*, 2267–2272.

(48) Perticaroli, S.; Ehlers, G.; Stanley, C. B.; Mamontov, E.; O'Neill, H.; Zhang, Q.; Cheng, X.; Myles, D. A. A.; Katsaras, J.; Nickels, J. D. Description of Hydration Water in Protein (Green Fluorescent Protein) Solution. *J. Am. Chem. Soc.* **2017**, *139*, 1098–1105.

(49) Nisbet, A. D.; Saundry, R. H.; Moir, A. J. G.; Fothergill, L. A.; Fothergill, J. E. The Complete Amino-Acid Sequence of Hen Ovalbumin. *Eur. J. Biochem.* **1981**, *115*, 335–345.

(50) Tokuyama, M.; Oppenheim, I. Dynamics of Hard-Sphere Suspensions. *Phys. Rev. E: Stat. Phys., Plasmas, Fluids, Relat. Interdiscip. Top.* **1994**, *50*, R16–R19.

(51) Banchio, A. J.; Nägele, G. Short-Time Transport Properties in Dense Suspensions: From Neutral to Charge-Stabilized Colloidal Spheres. *J. Chem. Phys.* **2008**, *128*, 104903.

(52) Nemoto, N.; Koike, A.; Osaki, K.; Koseki, T.; Doi, E. Dynamic Light Scattering of Aqueous Solutions of Linear Aggregates Induced by Thermal Denaturation of Ovalbumin. *Biopolymers* **1993**, *33*, 551–559.

(53) Weijers, M.; Visschers, R. W.; Nicolai, T. Light Scattering Study of Heat-Induced Aggregation and Gelation of Ovalbumin. *Macromolecules* **2002**, *35*, 4753–4762.

(54) Roosen-Runge, F.; Bicout, D. J.; Barrat, J.-L. Analytical Correlation Functions for Motion through Diffusivity Landscapes. *J. Chem. Phys.* **2016**, *144*, 204109.

(55) Voss, N. R.; Gerstein, M. 3V: cavity, channel and cleft volume calculator and extractor. *Nucleic Acids Res.* **2010**, *38*, W555–W562.

(56) Majorek, K. A.; Porebski, P. J.; Dayal, A.; Zimmerman, M. D.; Jablonska, K.; Stewart, A. J.; Chruszcz, M.; Minor, W. Structural and Immunologic Characterization of Bovine, Horse, and Rabbit Serum Albumins. *Mol. Immunol.* **2012**, *52*, 174–182.

(57) Harris, L. J.; Larson, S. B.; Hasel, K. W.; McPherson, A. Refined Structure of an Intact IgG2a Monoclonal Antibody. *Biochemistry* **1997**, *36*, 1581–1597.

(58) Loch, J. I.; Bonarek, P.; Polit, A.; Jabłoński, M.; Czub, M.; Ye, X.; Lewiński, K.  $\beta$ -Lactoglobulin interactions with local anaesthetic drugs - Crystallographic and calorimetric studies. *Int. J. Biol. Macromol.* **2015**, *80*, 87–94.

(59) van Eijck, L.; Gérard, L.; Frick, B.; Seydel, T.; Schober, H. A Case Study for Using Neutron Backscattering Instruments at Reactors in Inverted Time-of-Flight Mode. *Nucl. Instrum. Methods Phys. Res., Sect. A* **2012**, *672*, 64–68.

(60) Mamontov, E.; Herwig, K. W. A Time-of-Flight Backscattering Spectrometer at the Spallation Neutron Source, BASIS. *Rev. Sci. Instrum.* **2011**, *82*, 085109.

(61) Braun, M. K.; Wolf, M.; Matsarskaia, O.; Da Vela, S.; Roosen-Runge, F.; Sztucki, M.; Roth, R.; Zhang, F.; Schreiber, F. Strong Isotope Effects on Effective Interactions and Phase Behavior in Protein Solutions in the Presence of Multivalent Ions. *J. Phys. Chem. B* **2017**, *121*, 1731–1739.

(62) Bucciarelli, S.; Mahmoudi, N.; Casal-Dujat, L.; Jéhannin, M.; Jud, C.; Stradner, A. Extended Law of Corresponding States Applied to Solvent Isotope Effect on a Globular Protein. *J. Phys. Chem. Lett.* **2016**, *7*, 1610–1615.